Available online at www.sciencedirect.com
SCIENCE DIRECT®
Journal of Molecular Spectroscopy 220 (2003) 80–86
Journal of MOLECULAR SPECTROSCOPY
www.elsevier.com/locate/jms

Weak overtone transitions of N_2O around 1.05 μm by ICLAS-VECSEL☆

Y. Ding,[a,b] V.I. Perevalov,[c] S.A. Tashkun,[c] J.-L. Teffo,[d] S. Hu,[b] E. Bertseva,[a] and Alain Campargue[a,*]

[a] *Laboratoire de Spectrométrie Physique (associated with CNRS, UMR C5588), Université Joseph Fourier de Grenoble, B.P. 87, F-38402 Saint-Martin-d'Hères Cedex, France*
[b] *Laboratory of Bond-Selective Chemistry, University of Science and Technology of China, Hefei 230026, People's Republic of China*
[c] *Institute of Atmospheric Optics, SB, Russian Academy of Sciences, Tomsk 634055, Russia*
[d] *Laboratoire de Physique Moléculaire et Applications, C.N.R.S., Laboratoire associé à l' Université Pierre et Marie Curie, Case 76, Université Pierre et Marie Curie, 4 Place Jussieu, 75252 Paris Cedex 05, France*

Received 8 January 2003; in revised form 10 February 2003

Abstract

The weak overtone transitions of nitrous oxide, N_2O, have been investigated around 1.05 μm by Fourier Transform spectroscopy and intracavity laser absorption spectroscopy (ICLAS) using different vertical external cavity surface emitting lasers (VECSELs). Nine bands were rotationally analyzed revealing the occurrence of some local rotational perturbations. The interaction mechanisms and the perturbers are univocally assigned on the basis of the effective Hamiltonian model. In two cases, interpolyad couplings were evidenced indicating that the polyad version of the effective Hamiltonian has to be extended to include Coriolis and interpolyad anharmonic interactions.

1. Introduction

The aim of the present contribution is a further extension of the knowledge of the highly excited vibrational states of nitrous oxide using the intracavity laser absorption spectroscopy (ICLAS) [1–7]. In 1950, Herzberg and Herzberg investigated the absorption spectrum of N_2O with absorbing paths up to 4500 m atm and a spectrograph associated to photographic plates [8]. Some of their observations below 10 000 cm^{-1} were not reproduced up to now. Recently, the use of vertical external cavity surface emitting lasers (VECSELs) for ICLAS has opened the near infrared range for this highly sensitive absorption technique [9]. In a first contribution [7], we reported new observations between 9560 and 9980 cm^{-1}. In the present work, we could extend the spectral region investigated down to 8850 and up to 10 080 cm^{-1} using different VECSELs. This way, we could overlap the lower frequency region accessible to our ICLAS-Ti:sapphire spectrometer [6]. Three new very weak bands have been detected and the rotational analysis of four others was significantly improved. The rotational analysis will be presented with a particular emphasis on the newly observed rovibrational perturbations and a systematic comparison with the predictions of the effective Hamiltonian model.

2. Experiment

An overview of the Fourier Transform (FT) spectrum of N_2O in part of the region presently investigated by ICLAS is presented in Fig. 1. This spectrum was recorded in Hefei in order to help for an accurate wavenumber calibration of the ICLAS spectra. It was obtained using a Bruker 120 HR interferometer associated

☆ Supplementary data for this article are available on ScienceDirect.

* Corresponding author.
E-mail address: Alain.CAMPARGUE@ujf-grenoble.fr (A. Campargue).

0022-2852/03/$ - see front matter © 2003 Elsevier Science (USA). All rights reserved.
doi:10.1016/S0022-2852(03)00060-2

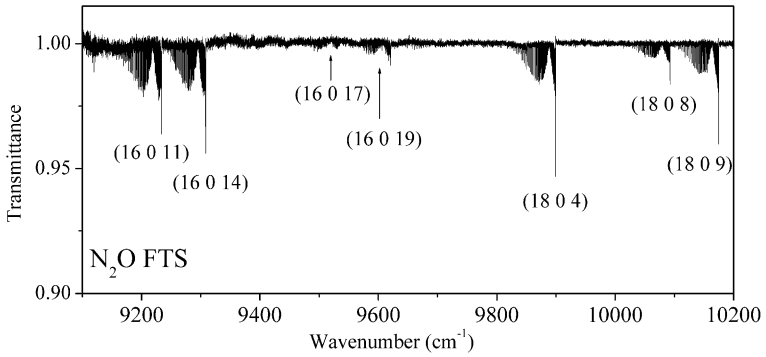

Fig. 1. Overview of the absorption FT spectrum of N_2O between 9100 and 10 200 cm^{-1} (resolution 0.028 cm^{-1}, pressure 206 hPa, absorption path length 105 m).

with a multipass cell. A tungsten source, quartz beam splitter and a Si-diode detector were used. The unapodized resolution was 0.028 cm^{-1} (0.9/maximum optical path difference). The scans (2342) were accumulated to improve the signal-to-noise ratio. The sample pressure and the absorption path length were $P = 206$ hPa and $l = 105$ m, respectively. The quality of the FT spectrum is illustrated by the observation of the very weak band at 9517.88 cm^{-1} which was not reported since the pioneer investigation of [8]. The FT spectrum was calibrated using water lines [10] present as impurity in the N_2O sample. We estimate the absolute wavenumber accuracy of the FT line positions to be about 0.003 cm^{-1}.

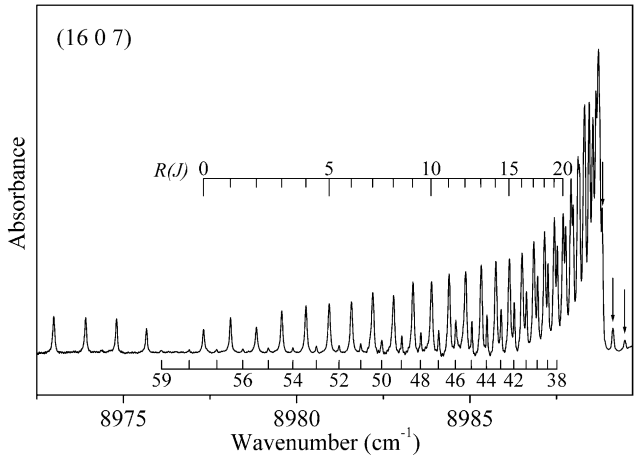

Fig. 2. ICLAS spectrum of N_2O in the range of the head of the R-branch of the Σ–Σ band centred at 8976.494 cm^{-1} corresponding to the excitation of the (16 0 7) state. The spectrum was recorded at a pressure of 49.4 hPa with an absorption equivalent path length of about 19.8 km. The (16 0 7) state is perturbed around $J' = 32$ through an anharmonic resonance with the (16 0 6) leading to the extra lines marked by arrows.

The ICLAS spectra were recorded in Grenoble with the experimental setup based on a VECSEL, previously described in [7,9] and applied recently to the spectroscopy of N_2O [7], H_2S [11], and OCS [12]. Three structures, with a quantum-well active region made up of GaAs-based semiconductors, were implemented in the present experiments (see [12] for more details). They allow for a continuous scan of the laser in the 8950–9100 and 9500–10 100 cm^{-1} spectral regions. The spectra were recorded with generation times up to 250 μs, leading to equivalent absorption path lengths up to 33 km. Depending on the band intensities, pressures between 13 and 140 hPa were adopted. Two examples of spectra in the region of the R branches of the (16 0 7)–(0 0 1) and (19 1 8)–(1 1 1) bands are presented in Figs. 2 and 3, respectively. Depending on the availability of FT line

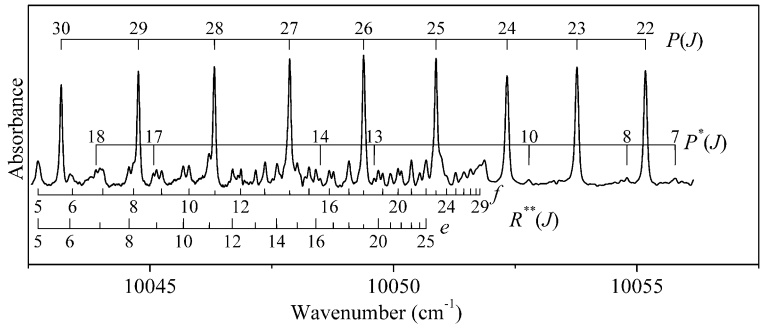

Fig. 3. ICLAS spectrum of N_2O in the range of the head of the R^{**}-branch of the Π–Π hot band centered at 10038.22 cm^{-1} reaching the (19 1 8) upper state. This band is superimposed with the P-branch of the strong Σ–Σ band at 10079.56 cm^{-1} and with the P-branch $P^*(J)$ of the weaker band at 10062.08 cm^{-1}. This spectrum was recorded at a pressure of 128 hPa with an absorption equivalent path length of 19.8 km.

positions, the ICLAS spectra were calibrated using either H_2O or N_2O line references. From the comparison of the wavenumber values obtained using independent reference lines, the accuracy of the ICLAS line positions is estimated to be around $0.005\,cm^{-1}$.

3. Rovibrational analysis

3.1. Vibrational assignment

The observed transitions can be easily assigned using the predictions of the effective Hamiltonian developed by Teffo et al. [13–16] based on a polyad structure resulting from the approximate relations between the harmonic frequencies $\omega_3 \approx 2\omega_1 \approx 4\omega_2$. The energy levels are uniquely labeled using the triplet $\{n_r = 2v_1 + v_2 + 4v_3,\ l_2, i\}$ where the index i increases with the energy. As discussed in [6], only states with a significant fraction of pure stretching states, $(v_1, v_2^{l_2} = 0^0, v_3)$, are detectable by absorption from the ground state. These bright states are weakly coupled by the anharmonic resonances, leading to a cluster structure among the observed levels. This structure was fully detailed in Table 3 of [6] and indeed all the newly observed levels are among those which were anticipated to be detectable in that paper. The vibrational assignment and fraction relative to the bright states are given for the presently studied Σ and Π levels in Tables 1 and 2, respectively. All the Σ states detected belong to the $\{n_r = 16$ and $18,\ l_2 = 0\}$ clusters.

3.2. Band by band rotational analysis

The band by band rotational analysis was performed using the standard procedure described in [6] for instance. The spectroscopic parameters retrieved from the fit of the line positions are presented in Tables 3 and 4 for the cold and hot bands, respectively. When available, we give in Table 3 the parameter values previously reported, which are found in close agreement with our measurements. All the wavenumbers and rotational assignments are available as supplementary data attached to the paper. An excellent agreement is also achieved between the retrieved values and the predictions of the *polyad* model [17] both for the vibrational term values G_v and the B_v rotational constants (see Table 1 and Table 2).

Five of the eight analyzed bands, corresponding to the (16 0 7), (16 0 10), (16 0 17), (18 0 8), and (17 1 7)

Table 1
The vibrational assignment for the presently studied Σ states and fractions relative to the bright states for the transitions from the ground vibrational state

$\{n_r, l_2, i\}$[a]	G_v (cm^{-1})		$\Delta B_v \times 10^2$ (cm^{-1})		Bright state	% Fraction[b]	Obs. – Pred.[c]
	Obs.	Calc.	Obs.	Calc.	$v_1, v_2^{l_2} = 0^0, v_3$		$\times 10^2$ (cm^{-1})
16,0,4	8877.052	8877.050	−1.1061	−1.1041	$20^03/40^02$	22.0/1.6	$\leqslant 1$
16,0,7	8976.494	8976.491	−1.3890	−1.3883	$20^03/00^04/40^02$	68.2/1.8/4.2	$\leqslant 1$
16,0,10	9108.390	9108.409	−0.8605	−0.8544	$40^02/60^01$	12.6/1.3	$-10 \leqslant\ \leqslant -4$
16,0,17	9517.880	9517.888	−0.9612	−0.9638	$60^01/40^02/80^00$	33.6/2.2/1.6	$\leqslant 1$
16,0,23	9975.200	9975.421	−1.0763	−1.0726	$80^00/60^01$	43.8/2.4	−23
16,0,24	10062.079	10062.183	−1.0213	−1.0169	80^00	12.8	−12
18,0,8	10079.561	10079.583	−1.2920	−1.2874	$30^03/50^02/10^04$	33.2/3.9/1.1	$\leqslant 1$

Note. The predicted vibrational terms G_v (calc.) and rotational constants B_v (calc.) were obtained from the *polyad model* of effective Hamiltonian [13–17]. For easier comparison, the ground state constant (0.419011 cm^{-1} [20]) was subtracted from the observed and predicted B_v values.

[a] Cluster labelling notation: $\{n_r = 2v_1 + v_2 + 4v_3, l_2, i\}$; i is the order number within the cluster increasing with the energy.

[b] Square of the expansion coefficient relative to the $(v_1, v_2^{l_2} = 0^0, v_3)$ bright state appearing in the eigenvector expansion with a fraction larger that 0.01.

[c] Estimation of the average difference between the observed and predicted [13–17] wavenumbers. The predicted wavenumbers have been obtained with the help of the polyad model of the effective Hamiltonian [17] except for the (16 0 17)–(0 0 1) and (17 1 6)–(0 0 1), (17 1 7)–(1 1 1) and (15 1 20)–(1 1 1) interacting bands (see Table 2) for which the nonpolyad model [17] has been used. In the case of the (16 0 10) level, this difference depends significantly on J and ranges between -10×10^{-2} ($J = 7$) and $-4 \times 10^{-2}\,cm^{-1}$ ($J = 42$).

Table 2
Vibrational assignment and fractions relative to the bright states for the Π states observed as upper state of transitions from the first excited vibrational state (0 1^1 0)

$\{n_r, l_2, i\}$	G_v (cm^{-1})		Bright state	% Fraction	Obs. – Pred.
	Obs.	Calc.	$(v_1, v_2^{l_2} = 1^1, v_3)$		$\times 10^2$ (cm^{-1})
17,1,7	9537.680	9537.322	$21^13/41^12/01^14$	56/3/2	−3
19,1,8	10627.394	10627.527	$31^13/51^12/11^14$	40/4/2	−16

See the footnotes of Table 1.

Table 3
Rovibrational parameters (in cm^{-1}) for the Σ–Σ cold bands of $^{14}N_2^{16}O$

$\{n_r, l_2, i\}$[a]	J_{pert}	State [b]	$\tilde{\nu}_0$	B_v	$D_v \times 10^7$	Lines[c]	*rms*[d]	Ref.
16 0 4		1 2^0 3	8877.051 8 (11)[f]	0.407 949 8 (22)	2.266 8 (79)	79 (83)	5.1	
			8877.054 8 (19)	*0.407 939 0 (96)*	*2.155 (94)*	*31 (57)*	*4.5*	[2]
16 0 7[e]	32	2 0^0 3	8976.478 0 (10)	0.405 112 1 (17)	1.518 4 (52)	98 (117)	6.2	
			8976.494 36 (66)	*0.405 120 9 (44)*	*1.373 (54)*	*48 (82)*	*2.1*	[2]
16 0 10[e]	26	3 2^0 2	9108.318 6 (29)[g]	0.410 406 (14)	3.92 (11)	21 (35)	7.0	
			9108.39	*0.410 34*				[8]
16 0 17[e]	35	6 0^0 1	9517.879 88 (44)	0.409 399 1 (37)	1.396 (56)	47 (63)	1.9	
			9517.92	*0.409 71*				[2]
16 0 23		8 0^0 0	9975.200 2 (16)[h]	0.408 248 2 (45)	1.996 (24)	66 (70)	6.7	
			9975.202 2 (23)	*0.408 240 0 (61)*	*1.957 (31)*	*38 (38)*	*6.8*	[7]
16 0 24		$<25\%$	10062.079 1 (25)	0.408 798 (*13*)	−0.79 (12)	34 (34)	6.3	
18 0 8[e]	45	3 0^0 3 and 1 4^0 3	10079.560 55 (91)	0.406 090 9 (23)	2.267 2 (89)	73 (86)	4.9	
			10079.556 5 (26)	*0.406 141 (13)*	*2.79 (13)*	*29 (52)*	*4.7*	[2]
			10079.559 70 18	*0.406 136 5 (12)*	*2.508 (15)*	*22 (28)*	*7.6*	[6]

The values between parentheses correspond to one standard deviation in the units of the last digit quoted. The values of the parameters obtained in previous studies are given in italics for comparison.

Note. The ground state constants were held fixed to the values of [20] ($B_v = 0.419\,011\,009$, $D_v = 1.761\,014 \times 10^{-7}\,cm^{-1}$).

[a] Cluster labelling notation: $\{n_r = 2v_1 + v_2 + 4v_3, l_2, i\}$; i is the order number within the cluster increasing with the energy.

[b] Upper state identified by the dominant $(v_1, v_2^{l_2}, v_3)$ state in the eigenvector expansion. Only states with a fraction larger than 25% are given.

[c] Number of fitted line positions with, between parentheses, the total number of rotationally assigned lines.

[d] Root-mean-square deviation (in $10^{-3}\,cm^{-1}$).

[e] Band affected by a rotational perturbation. The value of J_{pert} given in the second column, is that of the angular momentum corresponding to an energy level crossing with the perturber.

[f] The P branch of this band could not be recorded by ICLAS-VECSEL. We used the positions of the $P(J)$ lines measured on the FT spectrum.

[g] Only the P branch could be recorded. Lines with $J > 25$ are perturbed and were not included in the fit.

[h] P lines with $J > 21$ were taken from [7].

Table 4
Rovibrational parameters (in cm^{-1}) for the Π–Π hot bands of $^{14}N_2^{16}O$

$\{n_r, l_2, i\}$	J_{pert}	$\tilde{\nu}_0$[a]	B_v	$D_v \times 10^7$	$q \times 10^4$	Lines	*rms*[b]
17 1 7	*e*: 31; *f*: 25	8948.506 7 (13)	0.406 051 9 (80)	0.202 (95)	10.064 (55)	77 (110)	7.0
19 1 8		10038.219 9 (12)	0.406 706 5 (44)	2.042 (30)	15.862 (19)	107 (113)	6.8

The values between parentheses correspond to one standard deviation in the units of the last digit quoted.

Note. The constants of the (0 1^1 0) state were held fixed at the value found in [20]. See also the footnotes of Table 3.

[a] Band origin in cm^{-1}. Note that the vibrational term G_v is related to the band origin $\tilde{\nu}_0$ listed in Table 4 with the help of the following equation: $\tilde{\nu}_0 = (G_v - B_v) - (589.1873 - 0.4196)$.

[b] Root-mean-square deviation (in $10^{-3}\,cm^{-1}$).

states, were found to present local perturbations in their rotational structure, leading in some cases to the observation of extra lines. For instance, Fig. 4(a) shows the deviation from their unperturbed positions, for the energy levels of the (16 0 7) state affected by a perturbation around $J' = 32$ (J' is the angular momentum quantum number of the upper state of a transition). Similar perturbations by resonant dark states were evidenced in [6,7,18,19]. The main characteristics of the different local rovibrational perturbations observed in the considered spectral region are gathered in Table 5. In the following, we will discuss the identification of the perturbers and of the interaction mechanism performed on the basis of the effective Hamiltonian predictions. Two sets of effective Hamiltonian parameters have been used for these predictions. In most cases, the set of parameters of the effective Hamiltonian based on a polyad structure [13–16] was sufficient. But for the (16 0 17)–(0 0 1) and (17 1 7)–(1 1 1) bands affected by Coriolis and anharmonic interpolyad resonance interactions, respectively, we used a preliminary set of parameters of effective Hamiltonian which takes into account these interpolyad interactions. In both cases, the newly observed data were not included in the input data set used for the refinement of the effective Hamiltonian parameters. The approximate value of the deviations between the observed and predicted line positions are given in the last column of Tables 1 and 2. As the FT data of [2] have been included into the input file for the effective Hamiltonian parameters fitting, it is not surprising that the residuals between the observed and predicted line positions are very weak in the case of these four bands earlier observed in [2]. The line by line comparison included in the Supplement Material, shows that, for a given band, the differences depend very slowly on J as confirmed by the excellent agreement obtained between the observed and predicted values for the B_v rotational constants. Then the observed deviations which are all less than

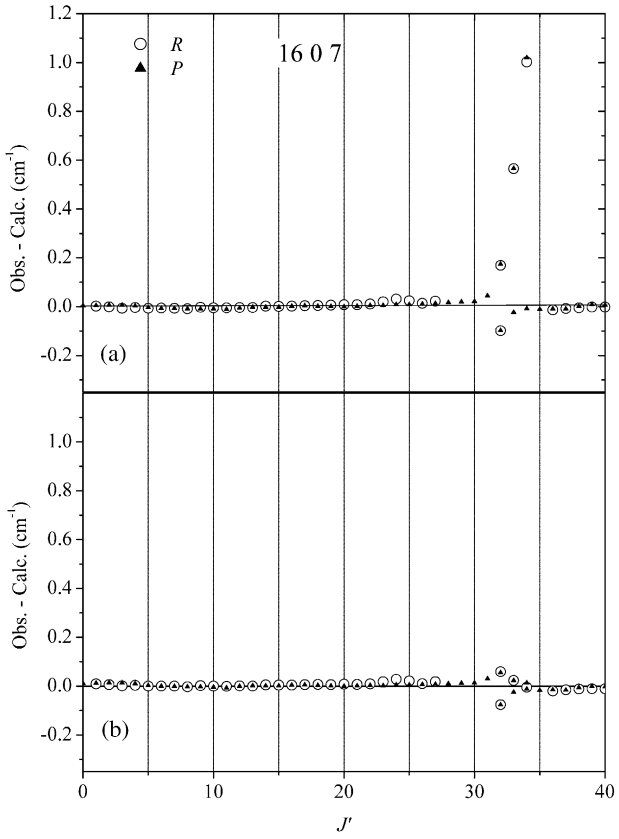

Fig. 4. (a) Shift of the energy levels of the (16 0 7) state from their unperturbed position. For each J' value, the observed energy levels of the upper states were obtained from $P(J'+1)$ transitions (triangle) and $R(J'-1)$ transitions (circle). The unperturbed energies were calculated from the rotational parameters of the (16 0 7) state given in Table 3. This state is affected by an anharmonic interaction around $J'=32$ with the (16 0 6) state. The plot also includes the energy levels of the perturbers observed through extra lines. (b) Similar plot as in (a) for the residuals between observed energy levels and those predicted using the effective Hamiltonian model [17].

Table 5
Summary of the local rovibrational perturbations observed in the $^{14}N_2^{16}O$ absorption spectrum investigated in this work

Bright state	Perturber	J_{pert}	Number of extra lines	Interaction type
(16 0 7)	(16 0 6)	32	6	anharmonic
(16 0 10)	(16 2 16)	26	0	anharmonic + l type
(16 0 17)	(17 1 6)	35	21	Coriolis
(17 1 7)	(15 1 20)	e: 31; f: 25	4	anharmonic
(18 0 8)	(18 2 13)	45	1	anharmonic + l type

$0.23\,cm^{-1}$, reflect the energy shifts of the vibrational term and are then mainly due to the vibrational part of the effective Hamiltonian. It is interesting to note the better data reproduction achieved by the non polyad model (as described below) in the case of the (17 1 7) level: the polyad model predicts the vibrational value $0.36\,cm^{-1}$ below its observed value while the non polyad model [2] reproduces the observed line positions within $-0.03\,cm^{-1}$.

3.3. Intrapolyad perturbations ($\Delta n_r = 0$)

The (16 0 7) level is perturbed by an anharmonic interaction with the (16 0 6) level leading to the appearance of six extra lines (see Fig. 2). The comparison of the reduced energy plots of Fig. 4 shows that the effect of the corresponding energy crossing is well predicted by the effective Hamiltonian [13–16].

The (16 0 10) and (18 0 8) levels are coupled by $|\Delta l_2| = 2$ interactions to the (16 2 16) and (18 2 13) states, respectively. The matrix elements of the corresponding l-type and anharmonic + l-type interactions are included into the effective Hamiltonian model and were given in Eq. (5) of [6] where the perturbation of the (18 0 8) state was analyzed in details. These resonance interactions lead to the activation of the $P(46)$ line of the "forbidden" band (18 2 13)–(0 0 1) which is indeed observed as extra line.

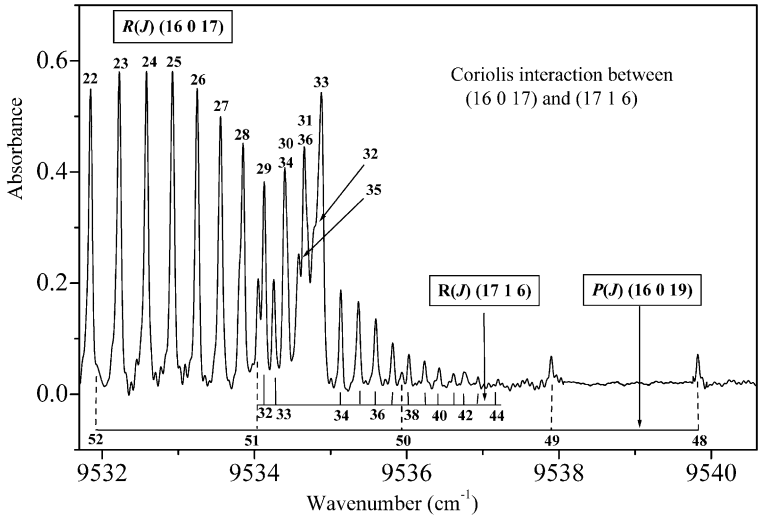

Fig. 5. The experimental spectrum of N_2O in the range of the head of the R-branch of the newly observed Σ–Σ band centered at 9517.88 cm^{-1}. This transition corresponds to an excitation of the (16 0 17) upper state which is perturbed around $J' = 35$ by a Coriolis interaction with the (17 1 6) state responsible for the observed extra lines. Several P lines of (16 0 19)–(0 0 1) band are also situated in the displayed region. The J assignment is given on the basis of the line positions predicted with the preliminary set of parameters of effective Hamiltonian which takes into account both anharmonic and Coriolis interpolyad resonance interactions [17]. The ICLAS-VECSEL spectrum was recorded at a pressure of 93.4 hPa with an absorption equivalent path length of 26.4 km.

3.4. Interpolyad perturbations ($\Delta n_r \neq 0$)

The present observation of high J rotational levels of the (16 0 17) state reveals that its rotational structure is perturbed around $J = 35$ by Coriolis interaction. A few other examples of perturbations due to Coriolis coupling ($\Delta n_r = 1$) have been previously discussed [7,18,19]. In the present case, the perturbation results from an energy levels crossing with the (17 1 6) state of the neighbour polyad. A number of extra lines are clearly apparent in the region of the head of the R branch displayed in Fig. 5. The global fitting of the N_2O line positions using the effective Hamiltonian model which includes both anharmonic interpolyad resonance interactions and Coriolis interpolyad resonance interactions is in a progress [17]. This model, called nonpolyad model, is an extension of the polyad model [13–16]. The extension has been performed by including the anharmonic interpolyad resonance interaction matrix elements, which are listed in [6], and the following interpolyad resonance Coriolis interaction matrix elements:

$$\left\langle V_1 V_2^{l_2} V_3 JK \middle| H^{\text{eff}} \middle| V_1 - 1(V_2 - 1)^{l_2 \pm 1} V_3 + 1 JK \pm 1 \right\rangle,$$

$$\left\langle V_1 V_2^{l_2} V_3 JK \middle| H^{\text{eff}} \middle| V_1 (V_2 - 3)^{l_2 \pm 1} V_3 + 1 JK \pm 1 \right\rangle,$$

$$\left\langle V_1 V_2^{l_2} V_3 JK \middle| H^{\text{eff}} \middle| V_1 + 2(V_2 - 1)^{l_2 \pm 1} V_3 - 1 JK \pm 1 \right\rangle.$$

As we could not scan our VECSELs in the region of the P branch of the (16 0 17) band, the GSCD method could not be applied and the line assignments of the (16 0 17)–(0 0 1) and (17 1 6)–(0 0 1) interacting bands, relies on the good agreement with the predictions of the interpolyad model of effective Hamiltonian [17].

The (17 1 7) state observed as upper state of the Π–Π hot band is found perturbed via interpolyad anharmonic interactions with the (15 1 20) state. The energy level crossing takes place at different J values for e and f parity levels: $J = 31$ and $J = 25$ for e and f levels, respectively. The rotational assignment was performed on the basis of the preliminary set of parameters of effective Hamiltonian [17]. The considered interpolyad ($\Delta n_r = 2$) anharmonic resonance interactions lead to the activation of four lines of the very weak (15 1 20)–(1 1 1) band due to an intensity borrowing from the stronger (17 1 7)–(1 1 1) band.

4. Conclusion

New experimental information about the rovibrational energy levels of N_2O near 1.05 μm has been obtained with an ICLAS set-up based on VECSELs. Five of the nine analyzed bands were found affected by local perturbations. In the case of intrapolyad energy crossing between bright and dark states, the corresponding rovibrational energy levels are satisfactorily accounted for in the frame of the cluster model [13–17]. However, the inclusion into the global effective Hamiltonian of interpolyad perturbations, of Coriolis or anharmonic types, is confirmed to be necessary to account for some of the observed perturbations. The preliminary set of parameters used for the interpolyad model [17] has however proved to give a key insight in the assignment process.

Acknowledgments

We are indebted to A. Garnache (CEM2, Université de Montpellier, France) for his contribution to the development of ICLAS-VECSEL in Grenoble and for providing some VECSEL samples. This work was supported by a collaborative project between CNRS and RFBR (PICS Grant 01-05-22002). V.I.P. and S.A.T. are also indebted to RFBR (Grant 00-07-90051). S.H. acknowledges a financial support from NSFC (Grant 2013007).

References

[1] A. Campargue, D. Permogorov, M. Bach, M. Abbouti Temsamani, J. Vander Auwera, M. Herman, M. Fujii, J. Chem. Phys. 103 (1995) 5931–5938.
[2] G. Weirauch, A.A. Kachanov, A. Campargue, M. Bach, J. Vander Auwera, M. Herman, J. Mol. Spectrosc. 202 (2000) 98–106.
[3] A. Campargue, D. Permogorov, Chem. Phys. Lett. 241 (1995) 339–344.
[4] A. Garnache, A. Campargue, A. Kachanov, F. Stoeckel, Chem. Phys. Lett. 292 (1998) 698–704.
[5] A. Campargue, Chem. Phys. Lett. 259 (1996) 563–567.
[6] A. Campargue, G. Weirauch, S. Tashkun, V. Perevalov, J.-L. Teffo, J. Mol. Spectrosc. 209 (2001) 198–206.
[7] E. Bertseva, A.A. Kachanov, A. Campargue, Chem. Phys. Lett. 351 (2002) 18–26.
[8] G. Herzberg, L. Herzberg, J. Chem. Phys. 18 (1950) 1551–1561.
[9] A. Garnache, A.A. Kachanov, F. Stoeckel, R. Houdré, J. Opt. Soc. Am. B 17 (2000) 1589–1598.
[10] L.S. Rothman, C.P. Rinsland, A. Goldman, S.T. Massie, D.P. Edwards, J.-M. Flaud, A. Perrin, C. Camy-Peyret, V. Dana, J.-Y. Mandin, J. Schroeder, A. McCann, R.R. Gamache, R.B. Wattson, K. Yoshino, K.V. Chance, K.W. Jucks, L.R. Brown, V. Nemtchinov, P. Varanasi, J. Quant. Spectrosc. Radiat. Transfer 60 (1998) 665–710.
[11] Y. Ding, O. Naumenko, S. Hu, Q. Zhu, E. Bertseva, A. Campargue, J. Mol. Spectrosc. (2003) 222–238.
[12] E. Bertseva, A. Campargue, Y. Ding, A. Fayt, A. Garnache, J.S. Roberts, D. Romanini, J. Mol. Spectrosc., in press.
[13] J.-L. Teffo, V.I. Perevalov, O.M. Lyulin, J. Mol. Spectrosc. 168 (1994) 390–403.
[14] O.M. Lyulin, V.I. Perevalov, J.-L. Teffo, J. Mol. Spectrosc. 174 (1995) 566–580.
[15] O.M. Lyulin, V.I. Perevalov, J.-L. Teffo, J. Mol. Spectrosc. 180 (1996) 72–74.
[16] E.I. Lobodenko, V.I. Perevalov, O.M. Lyulin, J.-L. Teffo, J. Mol. Spectrosc. 205 (2001) 239–247.
[17] S.A. Tashkun, V.I. Perevalov, J.-L. Teffo, to be published.
[18] C. Amiot, G. Guelachvili, J. Mol. Spectrosc. 51 (1974) 475–491.
[19] R.A. Toth, J. Mol. Spectrosc. 197 (1999) 158–187.
[20] M.D. Vanek, M. Schneider, J.S. Wells, A.G. Maki, J. Mol. Spectrosc. 134 (1989) 154–158.